Journal of Materials Chemistry A

PAPER

Cite this: J. Mater. Chem. A, 2015, 3, 2370

Received 8th November 2014
Accepted 8th December 2014

DOI: 10.1039/c4ta06045h

www.rsc.org/MaterialsA

The orientation dependence of the photochemical reactivity of $BiVO_4$†

Ratiporn Munprom, Paul A. Salvador and Gregory S. Rohrer*

$BiVO_4$ surfaces of all possible orientations have been used to photochemically reduce Ag^+ and oxidize Pb^{2+}. The surface orientations of grains, measured by electron backscatter diffraction, were correlated to the amounts of reduced and oxidized products on each surface. The results show that the photochemical reduction of Ag^+ is strongly favored on $BiVO_4$ (001) surfaces (indexed in group *I*2/*b*). However, Ag^+ can be reduced on all orientations, with the rate of reduction decreasing with increasing inclination from the [001] direction. The oxidation of Pb^{2+} is strongly favored on (*hk*0) surfaces perpendicular to (001). Surfaces within 50° of [001] have a much lower activity for the oxidation of Pb^{2+}. The results also show that reduction and oxidation reactions occur on complementary surfaces of $BiVO_4$ crystals.

1. Introduction

Bismuth vanadate, $BiVO_4$, is of interest for its potential application as a photoanode for water splitting.[1] With a bandgap of approximately 2.4 eV and a valence band edge at approximately 2.5 eV with respect to hydrogen evolution, $BiVO_4$ has the ability to oxidize water using holes generated by visible light.[1,2] There have been many efforts to modify $BiVO_4$ and improve its performance.[2–4] For example, substitutional dopants[5,6] have been added to increase the rate of charge carrier transport and co-catalysts[7–9] have been added to improve the oxidation kinetics. However, its performance is also limited by photogenerated electron–hole recombination.[10] Such loses can be ameliorated through the formation of a heterojunction that creates an internal field.[11] Catalysts with junctions between Co_3O_4 and $BiVO_4$ have shown notable improvements in the rates of oxidation reactions.[11–14] It is also possible to separate charges using internal polarizations and charged surfaces,[15–20] but the importance of these phenomena in $BiVO_4$ have not yet been fully explored.[21]

Morphological control has been suggested as another way to limit recombination in $BiVO_4$ crystals. It is known that different surfaces of the same crystal are able to promote different reactions.[22,23] In the case that one surface promotes reduction and the other oxidation, it would be possible to create particles that spatially separate the oxidation and reduction reactions.[24] Before discussing prior results on the orientation dependence of the reactivity of $BiVO_4$, it is necessary to make some comments about the crystallography.

$BiVO_4$ can crystallize in a tetragonal zircon structure, a tetragonal scheelite structure, or a monoclinic fergusonite structure. This latter structure is sometimes referred to as "monoclinic scheelite" because of its similarity to the higher symmetry structure. Of these, the monoclinic structure has been reported to be the most photochemically active.[25] The equilibrium structure at room temperature and pressure is fergusonite and this is the structure of $BiVO_4$ that will be discussed in this paper.[26] $BiVO_4$ in the tetragonal scheelite structure ($I4_1/a$, $a = 5.1470$ Å $c = 11.7216$ Å)[26] transforms to the monoclinic fergusonite structure ($I2/b$, $a = 5.1956$ Å, $b = 5.0935$ Å, $c = 11.704$ Å, $\gamma = 90.383°$)[26] through a small ferroelastic distortion below 255 °C. This transformation alters the cell parameters by less than 1% and creates a ferroelastic domain structure.[27] While the ferroelastic domains also affect the photochemical reactivity,[21] the current paper focuses on the effect of crystal orientation and largely ignores the effect of the domains.

The indices used to identify surface planes depend on the symmetry, choice of axes, and unit cell. Several different choices have been made in the past for $BiVO_4$ and, for comparison with that work, it is necessary to be clear about the convention used here. If the unit cell is selected according to modern crystallographic conventions, the diad is along *b* (the longest axis) and the space group is *C*2/*c* (no. 15). However, if one assigns the diad axis to *c*, to preserve the relationship between the monoclinic cell and the more idealized tetragonal structure, then the appropriate name for the group is *I*2/*b*. We make the latter choice for consistency with our electron backscatter diffraction (EBSD) experiments. In all comparisons to previous work, we shall use indices in *I*2/*b*, even when the previous authors indexed the cell in *C*2/*c* or some other choice.

Wang *et al.*[28] showed that the rate of oxygen evolution during illumination in visible light increases with the area of the (001)

Department of Materials Science and Engineering, Carnegie Mellon University, 5000 Forbes Ave., Pittsburgh, PA 15213-3890, USA. E-mail: gr20@andrew.cmu.edu

† Electronic supplementary information (ESI) available. See DOI: 10.1039/c4ta06045h

facet. Later, the reactivity of polygonal $BiVO_4$ particles bounded almost entirely by (001), (101) and (011) facets was studied.[29,30] Marker reactions that leave insoluble products on the surface where oxidation and reduction occur were used to show that reduction was promoted on (001) facets and oxidation was promoted on (101) and (011) facets. This was attributed to small differences in the valence and conduction band edges at the two surfaces that promoted electron transfer to (001).[30] More detailed calculations suggest that there are several competitive factors and that a single simple parameter might not be sufficient to describe the orientation dependence of the reactions.[31]

The purpose of the present paper is to describe the complete orientation dependence of the photochemical reactivity of $BiVO_4$. Whereas the previous work[29–31] concentrated on polygonal particles exposing only (001), (101), and (011) facets, we employ a method that allows us to compare the reactivities of all possible orientations. We have produced dense ceramic samples with large grains, essentially the same as those previously used to study the effect of the ferroelastic domains.[21] The polished surface of the polycrystal simultaneously exposes all possible crystal orientations. The orientations are measured by EBSD, and marker reactions that leave insoluble products on the surface at the site of the reaction are then used to explore the preferences among the different surfaces for reduction and oxidation. The results make it possible to propose an ideal particle shape to promote charge carrier separation.

2. Experimental

Monoclinic $BiVO_4$ was prepared by a conventional solid-state reaction using a stoichiometric mixture of Bi_2O_3 (99.975% pure) and V_2O_5 (99.99% pure) powders.[21] The mixture (~12.5 g) was ball-milled overnight in a 125 ml plastic bottle using yttria stabilized zirconia grinding media and 15 ml of ethanol as a lubricant. After ball milling, the mixture was dried in air at 85 °C and then heated to 650 °C in air for 2 h to complete the reaction. The reacted powder was then manually ground in a mortar and pestle to reduce the particle size. The powder was mixed with 5 wt% of PVA as a binder and compressed in a 1 cm-diameter cylindrical stainless steel die with 59 kN of force to form a pellet with a thickness of ~3 mm. The pellet was annealed at 500 °C in air for 6 h to decompose the binder and any other organics, and then sintered at 800 °C in air for 12 h. Powder X-ray diffraction (see Fig. S1†) was used to verify that the product had the structure of monoclinic fergusonite, as expected for $BiVO_4$ at room temperature. The optical reflectance spectrum of the material is presented in Fig. S2.†

The surface was prepared by lapping, polishing and annealing. First, the samples were lapped using SiC abrasive papers (initially with 320 grit and followed by 400, 600, 800 and 1200 grit, respectively) to get a flat surface. Afterwards, they were consecutively polished with 1 μm, 0.3 μm and 0.05 μm alumina suspensions, respectively. Each lapping step required several minutes, while each polishing step took 30–60 min. Finally, the sample was annealed in air at 300 °C for 1 h to repair surface damage accumulated during the polishing.

Electron backscatter diffraction (EBSD) was used to determine the orientations of the crystals at the surface of the sample. EBSD measurements were carried out in a Quanta200 scanning electron microscope (FEI company) equipped with an orientation imaging microscopy (OIM) system that used a Hikari charge coupled device detector to collect the diffraction patterns. TSL software was used to analyze the surface orientations and generate an orientation map of the scanned area. As noted in the first section, the room temperature structure of $BiVO_4$ is monoclinic, with space group $I2/b$ and lattice parameters $a = 5.1956$ Å, $b = 5.0935$ Å, $c = 11.704$ Å, $\gamma = 90.383°$.[26] Because a and b differ by only 2%, and γ is nearly equal to 90°, the cell is approximately tetragonal, analogous to the higher temperature scheelite-structured parent phase. Therefore, to simplify the orientation measurements, we assumed that $BiVO_4$ has a tetragonal unit cell with lattice parameters $a = 5.1509$ Å and $c = 11.73°$ and indexed the EBSD patterns in Laue group $4/m$. The most important artifacts of this assignment are that the longest axis is [001] and the crystallographically distinct (100) and (010) monoclinic surfaces become indistinguishable. Orientation maps were recorded over 200 μm × 200 μm areas with a step size of 1 μm. Several 'clean-up' procedures were used to minimize the number of un-indexed or incorrectly indexed pixels. First, a grain dilation clean-up was applied using a 5° tolerance angle, a 10 pixel minimum grain size, and a so-called multiple row requirement. The fraction of points changed in this clean-up process was about 19%. Next, an average orientation was assigned to each grain, where a grain is defined with a tolerance angle of 5°. To verify that this simplification of the symmetry did not impact the results, several experiments were conducted using the monoclinic cell and point symmetry $2/m$. Examples of these results are included in the ESI (see Fig. S3†). Both tetragonal and monoclinic indexing schemes yield consistent orientations for all grains. Also, there were no detectable differences between the reactivities of the (100) and (010) surfaces. As such, use of the simpler tetragonal system is appropriate.

The photochemical reactivity of individual grains was evaluated using reactions that left a solid product on the surface that could then be observed microscopically. Aqueous solutions of 0.115 M $AgNO_3$ (99.85% pure) were used for the photochemical reduction of Ag^+ to Ag^0.[32,33] Aqueous solutions of 0.115 M $Pb(NO_3)_2$ (99.6% pure) were used for the photochemical oxidation of Pb^{2+} to Pb^{4+}.[34,35] For the case of the Pb^{2+} bearing solutions, an electron acceptor (IO_3^-) was added to the solution to promote the reaction. The electron acceptor was added to the Pb^{2+} bearing solution as 0.23 M $NaIO_3$ (>99% pure); because some insoluble $Pb(IO_3)_2$ always formed after the addition of the $NaIO_3$, the mixture was filtered to remove the precipitate and the clear supernate was used in the experiment. The solutions were not degassed and were stored in sealed glass containers for later use in experiments. These two marker reactions have been employed extensively in previous work on photochemically active oxides,[22–24,34,36] including $BiVO_4$.[21,29,30] Schematic energy level diagrams for silver reduction and lead oxidation are shown in Fig. 1. The value of the bandgap was taken to be 2.4 eV and the conduction band edge was assumed to be at 0.1 eV[2].

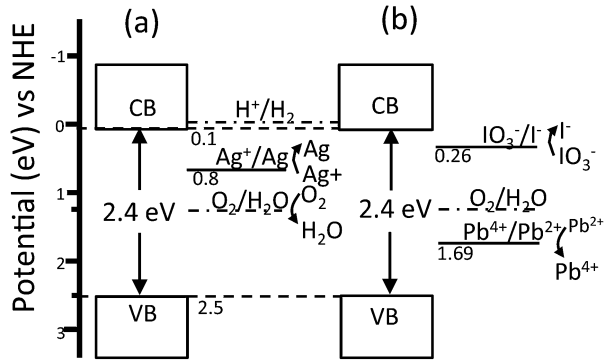

Fig. 1 Energy level diagram showing the band edge positions and redox potentials (a) in $AgNO_3$ solution, where Ag^+ accepts electrons for reduction, and (b) in $Pb(NO_3)_2$ solution where IO_3^- accepts electrons while Pb^{2+} accepts holes.[37]

The same procedure was used for each photochemical experiment. An O-ring was placed on the sample surface to create a reservoir that was then filled with the metal-bearing solution. The top was sealed with a quartz cover slip that was held in place by capillarity. Illumination was provided by a blue light-emitting diode (LED, wavelength of 470 nm, 2.64 eV) placed just above the sample and in contact with the cover slip. The LED was operated at 5 V with a current of 750 mA. $BiVO_4$ has different activities for the different reactions, so the exposure time was optimized so that the reaction product was easy to detect in atomic force microscope images, but not so prevalent that the large topographic variations complicated the imaging. The exposure times were 1 min and 20 min for the $AgNO_3$ and $Pb(NO_3)_2$ solutions, respectively. Reduction and oxidation reactions were carried out on the same samples, on the same areas. After Ag^+ reduction, the sample surfaces were ultrasonically cleaned in acetone and methanol, before the oxidation reaction. By comparing AFM images before and after the cleaning (see Fig. S4†), it is clear that most of the silver is removed, but it is likely that a small amount remains, especially in the topographically depressed areas such as grain boundary grooves, scratches, and pores. To verify that the reaction products are formed through photochemical processes, control experiments were performed in which the samples were immersed in the metal bearing solutions for 30 min, but without illumination. In these cases, no reaction products were found on the surface.

The surface topography of the same areas in the orientation maps, before and after the reactions, was measured by atomic force microscopy (AFM) using a SolverNext NT-MDT scanning probe microscope operated in tapping mode. Features that appeared on the surface after the reaction were assumed to be the reaction product, as demonstrated in previous work.[21,30] Because it is topographically higher than the surrounding surface, the reaction products appear as bright contrast in the AFM images. The relative reactivities of different surfaces were determined by the relative heights of the deposits compared to the surface before the reaction.[38] The effect of orientation on the reactivity was investigated by correlating the surface orientation with the measured reactivity.

3. Results

The effect of Ag^+ reduction on the surface is illustrated in Fig. 2. The AFM images in Fig. 2(a) and (b) show the surface topography before and after reduction, respectively. In Fig. 2(a), the different heights of the grains lead to abrupt changes in contrast at the grain boundaries and the striped contrast within the grains corresponds ferroelastic domains. While these domains obviously influence the reactivity,[21] this paper focuses on the effect of grain orientation. By comparing the images in Fig. 2(a) and (b) it is clear that much more silver deposits on some grains than others; this is confirmed by the topographic profiles in Fig. 2(c) and (d). On the surface of the grain with low reactivity (denoted by L), the silver deposits have an average height of ~12 nm, while the height of the reaction product on the highly reactive surface (denoted by H) is ~70 nm. Note that in all of the profiles, the heights of separate Ag particles are relatively consistent within ± 10 nm.

The images in Fig. 3 compare the topography of the surface after the reduction of Ag^+ to the grain orientations measured by EBSD. It should be noted that Fig. 3(a) is a montage of smaller images, so there are some horizontal and vertical discontinuities in the contrast. To illustrate the correspondence between the images, the same two grains are outlined with a white line. Based on the contrast in the AFM image, the reduction of silver is clearly heterogeneous. There are two types of heterogeneities. The first is a grain-by-grain reactivity that changes abruptly at the grain boundaries. The present paper focuses on this grain-to-grain heterogeneous reactivity. Other heterogeneities arise from the presence of polishing scratches and ferroelastic domains. The polishing scratches are long straight features that traverse grains and boundaries uninterrupted and one is labeled 'PS'. The ferroelastic domains are parallel stripes contained within grains. There are also occasional "islands" of higher reactivity that occur within grains (examples marked with an "x" in Fig. 3(a)). These features will not be discussed here and we focus instead on the variations related to grain orientation, away from these islands. From a qualitative perspective, the trend in reactivity with orientation seems obvious. The grains with high reactivity in Fig. 3(a) have orientations near (001) in Fig. 3(b). Similarly, the grains with low reactivity have orientations that are closer to (*hk*0), roughly perpendicular to (001).

To quantify the orientation dependence of the reduction of silver, about a hundred grains were evaluated according to the heights of the silver deposited on the surface. To measure the height, a height profile was extracted from each grain, as illustrated in Fig. 2. Areas classified as highly reactive had silver particles whose average heights were greater than 20 nm. Areas classified with low reactivity had silver particles whose average heights were less than 20 nm. To illustrate how grains in Fig. 3 were classified, low reactivity grains are labeled 'L' and high reactivity grains are labeled 'H'. The orientation distribution of low- and high-reactivity grains is shown in Fig. 4. The plots show

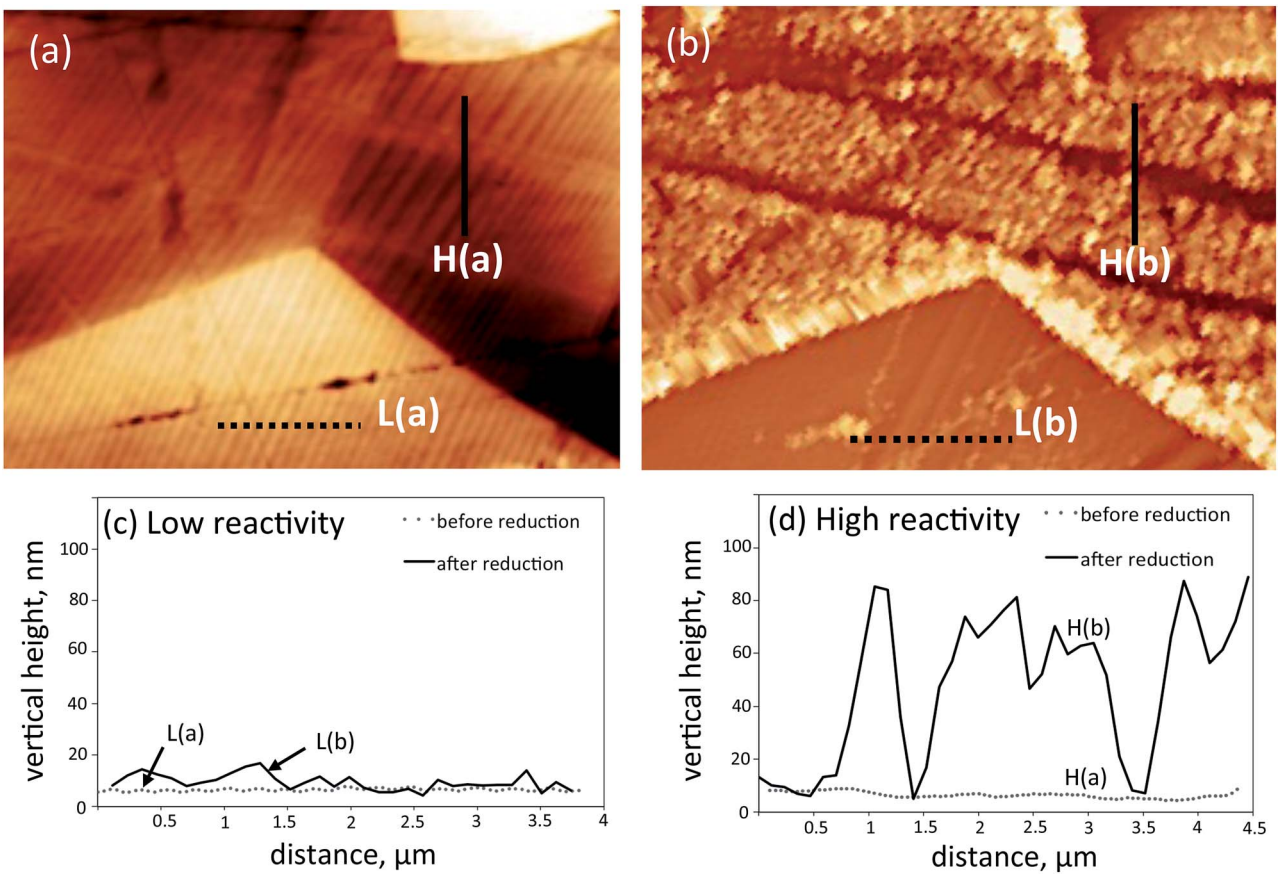

Fig. 2 Silver reduction on the $BiVO_4$ surface (a) topography before reduction and (b) topography after reduction. The height profile of the low reactivity grain ('L' line) and one of the high reactivity grain ('H' line) are shown in (c) and (d), respectively. The black-to-white contrast is 12 nm in (a) and 90 nm in (b). The field of view is 10 μm × 15 μm.

that there are no low-reactivity grains within 40° of [001]. The high-reactivity grains appear to be clustered near [001], and fewer are found as the inclination from [001] is increased. The average heights of the silver as a function of orientation are shown in Fig. S5.† The data in Fig. 5 indicates that as the angle between the surface orientation and [001] increases, there are fewer grains whose average heights of silver particles exceed 20 nm.

To quantify the distribution of high and low reactivity grains, we compare the orientations to those expected in a random distribution. Specifically, we divide the fraction of observations in 10° ranges by the fraction that would be found in a random orientation distribution; the resulting units are multiples of a random distribution (MRD). The results are illustrated in Fig. 5. In the range between 0 and 10° from [001], grains that reduced silver are four times more likely than random and between 80° and 90° from [001], grains that reduced silver were five times less likely than expected at random. Similarly, there are no low reactivity grains within 40° of [001], but from 80° to 90° from [001], they are more than twice as likely as in a random distribution. So, while all grain orientations can reduce some silver, grains within 40° of [001] reduce much more in the same amount of time. Note that the orientations of the facets on the polygonal crystals studied by Li *et al.*[30] are indicated on the horizontal axis. The red circle at zero indicates the orientation of the facet active for reduction and the blue square indicates the facet that was inert for reduction and active for oxidation in Li's[30] study.

The orientation dependence of the oxidation of Pb^{2+} was determined the same way that the orientation dependence of the reduction reaction was determined. The topography of the $BiVO_4$ surface after illumination in an aqueous $Pb(NO_3)_2$ solution is shown in Fig. 6(a) and an orientation map of the same area is shown in Fig. 6(b). Overall, the oxidized reaction product (in Fig. 6(a)) appears as white contrast, representing features that are 50–70 nm in height. Ignoring irregularities such as the polishing scratches, it is clear that there are sometimes abrupt changes in the amount of reaction product at grain boundaries, with some grains being reactive (having a large amount of oxidized material on the surface) and others being almost unreactive (very little reaction product on the surface). When one compares the orientation map with the distribution of reaction product, it is clear that grains with surface orientations near (001) are unreactive, while the more reactive grains are roughly perpendicular to (001). Three examples of high and low reactivity grains are outlined and labeled H and L, respectively.

To demonstrate the orientation dependence of the reactivity, the orientations of 54 reactive and 36 unreactive grains are

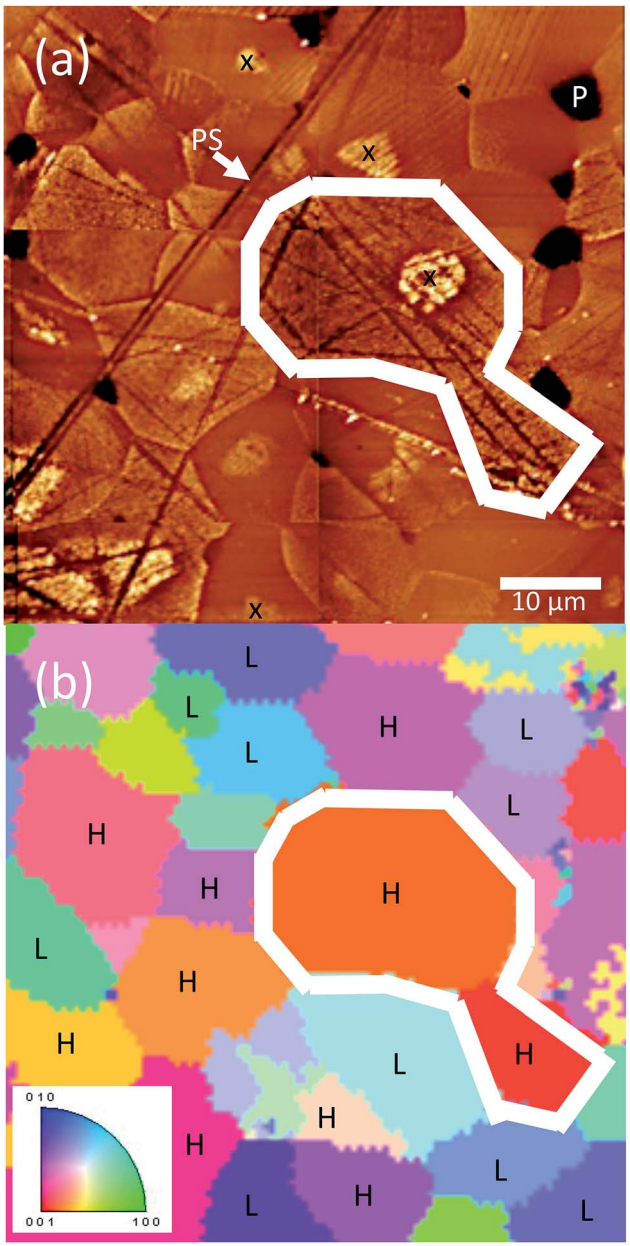

Fig. 3 (a) Topographic AFM image after Ag^+ reduction. The black-to-white vertical contrast is 196 nm. (b) Orientation map of the same area. The color key is shown in the inset. The field of view is 60 μm × 60 μm. In (a), an example of a polishing scratch is marked with "PS" and a surface pore with "P".

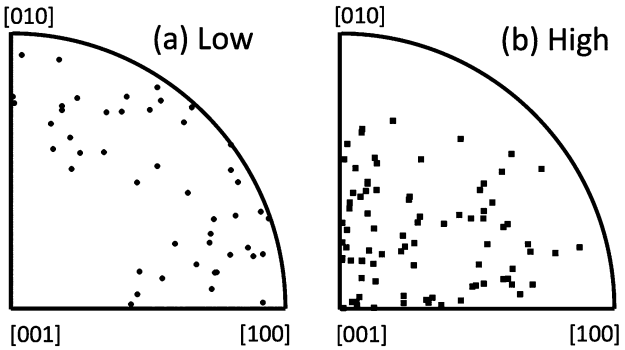

Fig. 4 Orientations of grains on the $BiVO_4$ surface that were classified as low (a) and high (b) reactivity for the photochemical reduction of Ag^+. Each point corresponds to an observed grain and the points are plotted in stereographic projection.

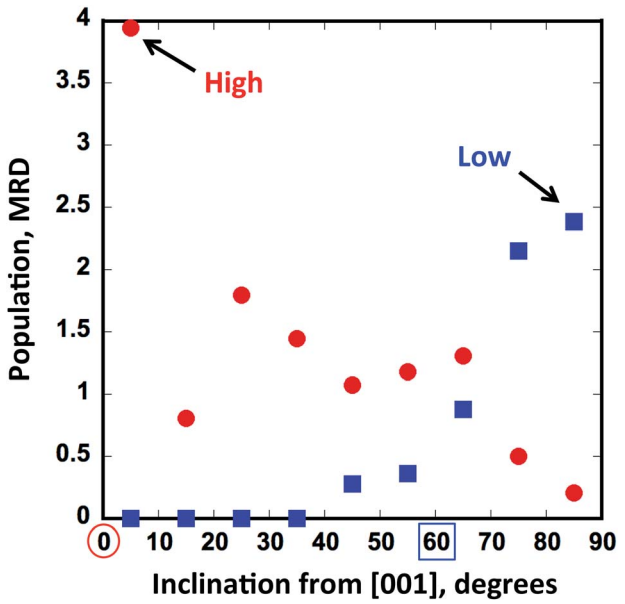

Fig. 5 The orientation distribution of grains with high and low reactivity, as a multiple of a random distribution. The red circles are for the high reactivity grains and the blue squares are for the low reactivity grains.

plotted on the stereographic projections in Fig. 7(a) and (b), respectively. From these observations, it is clear that all of the reactive grains have orientations that are at least 50° from [001] and all of the unreactive grains have orientations that are closer to [001]. Note that this is roughly opposite of what was observed for the reduction reaction. In other words, grains with orientations near [001] are more active for reduction and grains with orientations closer to (*hk*0) are more active for oxidation.

The topography of the same area of the $BiVO_4$ surface after reduction and oxidation are compared in Fig. 8. The grains that reduce the most Ag^+ are inactive for the oxidation of Pb^{2+}, and those that oxidize Pb^{2+} are less active for Ag^+ reduction, indicating (001) and (*hk*0) orientations have complementary reactivity. However, it should be noted that there is a range of orientations that have some activity for both reactions. In Fig. 9, the populations of grains that have a high reactivity for oxidation and reduction are compared. The population of the grains that have a high reactivity for reduction is centered at [001] and the population of grains that have a high reactivity for oxidation is centered perpendicular to this direction, at (*hk*0). At the limiting ranges of the orientations, a grain's reactivity is almost exclusively reduction or oxidation. However, for a range of orientations between these limits, both oxidation and reduction are possible. As in Fig. 5, the orientations of the facets on the

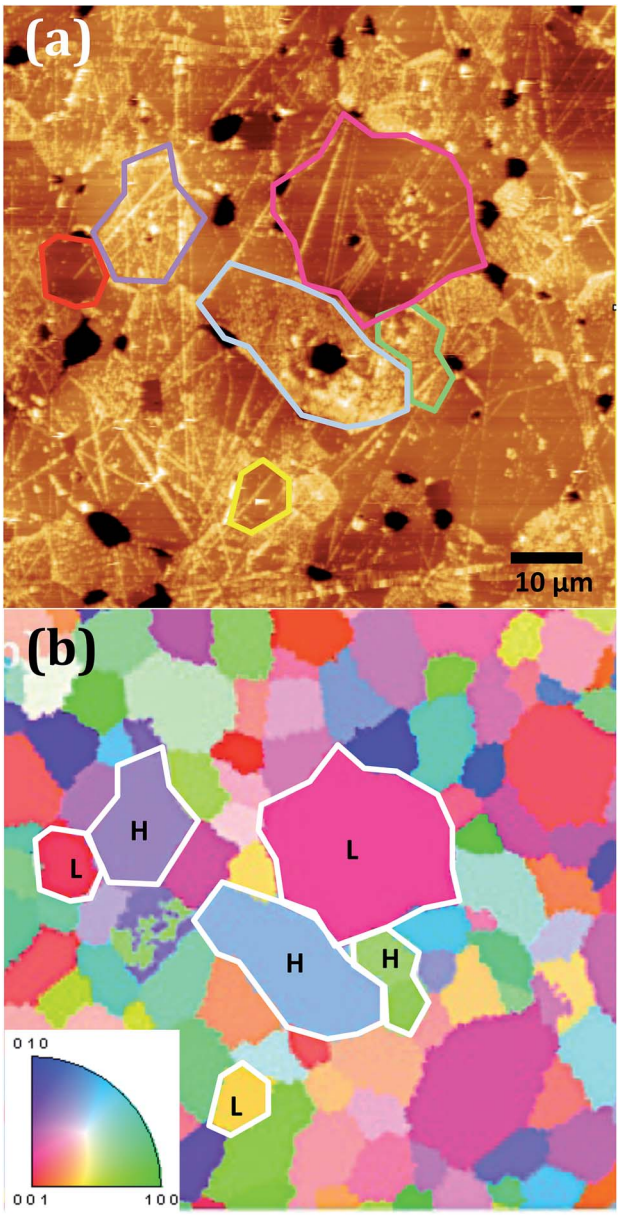

Fig. 6 (a) Topographic AFM image of the $BiVO_4$ surface after a photochemical reaction in a $Pb(NO_3)_2$ solution. The vertical height from dark-to-light contrast is 220 nm. (b) Orientation map of the same area colored by orientation according to the inset. The field of view is 90 μm × 90 μm.

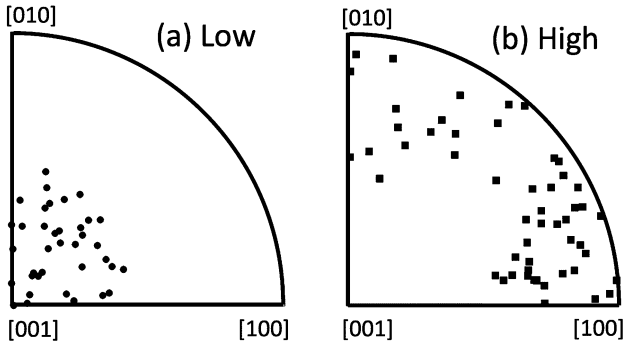

Fig. 7 Orientations of grains on the $BiVO_4$ surface that were classified as low (a) and high (b) reactivity for the photochemical oxidation of Pb^{2+}. Each point corresponds to an observed grain and the points are plotted in stereographic projection.

polygonal crystals studied by Li *et al.*[30] are indicated on the horizontal axis. The present results are consistent with the results from the polygonal crystals, bearing in mind that the current experiment probes all orientations. For example, while Li's result indicate that (101) is inert for reduction (60° from [001]), the current results indicates that there are other surfaces 60° from [001] that are able to reduce some silver.

4. Discussion

The photochemical reactivity of $BiVO_4$ observed here is consistent with that reported by Li *et al.*[30] The prior work considered polygonal particles bounded by (001), (101), and (011) faces. The (101) and (011) faces were not discriminated in the previous work and appeared to have the same reactivity, an observation consistent with the current work. Li *et al.*[30] found reduction exclusively on the (001) surface and oxidation exclusively on the other two facets. Our results agree in the sense that (001) favors reduction and surfaces inclined by more than 50° favor oxidation. However, the reactivity was not exclusive in our experiments. Surfaces close to (001) had the highest reactivity, but all surfaces could reduce some Ag^+ (see Fig. 4), even if it was a small amount. By examining all possible orientations, it was found that it is the surfaces perpendicular to (001), those with indices of the type (*hk*0), that have the highest photochemical reactivity for the oxidation of Pb^{2+}. These surfaces were not available on the particles studied in the previous work.[29,30]

There are a few possible experimental differences between the current work and the previous work[29,30] that should be mentioned. For example, the surfaces on the ceramic specimens have much larger areas for each orientation than on the small particles; the grains are usually several tens of microns in diameter. It is difficult to imagine that photogenerated electron–hole pairs travel to different grains to react, whereas it is possible that they travel to different facets in sub-micron sized crystals. It is more likely that a surface that reduces Ag^+ is also oxidizing water at the same rate and a surface that oxidizes Pb^{2+} is also reducing IO_3^- at the same rate. This is made possible by the ferroelastic domains in the grains, which appear polar in piezoforce microscopy images, providing closely spaced sites for oxidation and reduction on all grains.[21] The more exclusive oxidation and reduction behavior on the small single crystals might be because the oxidation and reduction sites are separated by only a few hundred nanometers and the photogenerated carriers can traverse these distances. It should also be noted that other defects such as grain boundaries do not appear to influence reactivity further than a few nm from their location.

The mechanism for the anisotropic reactivity is not known with certainty. Previous studies of the anisotropic photochemical reactivity of oxides have suggested the importance of both bulk and surface properties. For example, Giocondi *et al.*[39] attributed the anisotropic photochemical activity of $SrTiO_3$

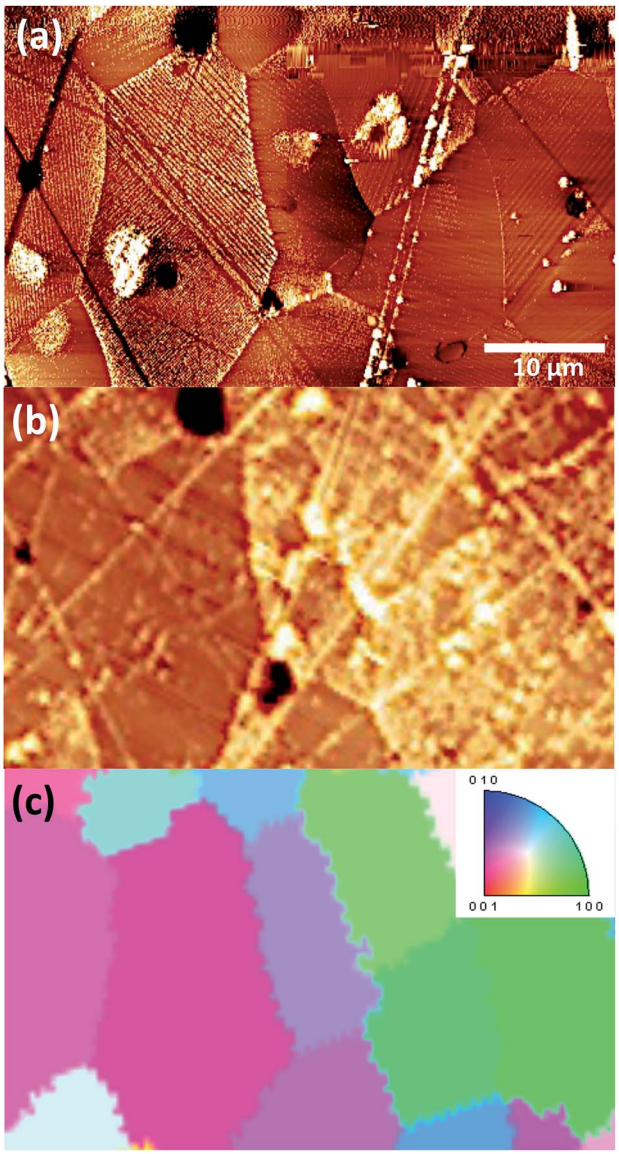

Fig. 8 Topographic AFM image of the $BiVO_4$ surface after a photochemical reaction (a) after reduction and (b) after oxidation. (c) An orientation map of the same area colored by orientation. The topographic vertical contrasts of (a) and (b) are 110 and 220 nm, respectively. The field of view is 30 μm × 50 μm.

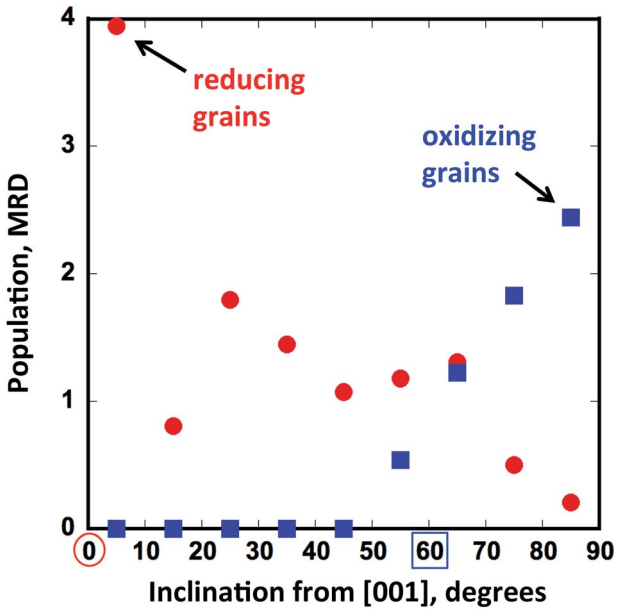

Fig. 9 The orientation distribution of grains with a high reactivity for reduction (red circles) and oxidation (blue squares), as multiples of a random distribution.

polycrystals to differences in the energies needed to create electron–hole pairs with momentum along different crystallographic directions. They also argued that surface polarity played a role.[36] Recent studies of rutile conclude that anisotropic charge carrier mobility explains anisotropic photochemical reactivity.[40] Past studies of the anisotropic properties of hematite proposed that higher photocurrent densities on prismatic surfaces (in comparison to basal surfaces) was the result of greater electronic conductivity parallel to the basal plane. This factor could improve the electron–hole separation and therefore decreases recombination, leading to greater photocurrent densities. The conductivity may also play a role in $BiVO_4$. Based on DFT calculations, it has been reported that electrons and holes have a higher drift velocity in the direction of the (001) surface.[31] This would bring more of the majority carrier (electrons) to the (001) surface and promote reduction. Under these circumstances, the minority carrier (hole) population would be very low. The localization of oxidation reactions to perpendicular surfaces may be because the comparatively lower electron populations at these surfaces leads to longer hole lifetimes.

The findings described here make it possible to propose an ideal particle shape for a $BiVO_4$ catalyst. The particle would not have to be fully faceted. Instead, it could be cylindrical with two flat {001} faces (the best surfaces for reduction) and any combination of (*hk*0) surfaces which are all active for oxidation. The relative areas of the surfaces would be adjusted so that one half of the reaction would not limit the other. For example, because reduction is relatively fast in the present experiments compared to oxidation, the particle would be acicular, with relatively larger lateral surfaces. On the other hand, if the reduction half reaction were sluggish compared to the oxidation half reaction, a flatter disc shaped particle would be desirable.

5. Conclusions

The photochemical reduction of Ag^+ is strongly favored on $BiVO_4$ (001) surfaces. However, Ag^+ can be reduced on all orientations, with the rate of reduction decreasing with increasing inclination from the [001] direction. The oxidation of Pb^{2+} is strongly favored on (*hk*0) surfaces that are perpendicular to (001). Surfaces within 50° of [001] have a much lower activity for the oxidation of Pb^{2+}. The ideal $BiVO_4$ particle to promote photochemical reactions would be comprised of perpendicular (001) and (*hk*0) surfaces with relative areas that balance the reduction and oxidation rates.

Acknowledgements

The authors acknowledge the support of National Science Foundation grant DMR 1206656.

Notes and references

1 A. Kudo, K. Ueda, H. Kato and I. Mikami, *Catal. Lett.*, 1998, **53**, 229–230.
2 Y. Park, K. J. McDonald and K.-S. Choi, *Chem. Soc. Rev.*, 2013, **42**, 2321–2337.
3 Z.-F. Huang, L. Pan, J.-J. Zou, X. Zhang and L. Wang, *Nanoscale*, 2014, **6**, 14044–14063.
4 F. E. Osterloh, *Chem. Soc. Rev.*, 2013, **42**, 2294–2320.
5 F. F. Abdi, N. Firet and R. van de Krol, *ChemCatChem*, 2013, **5**, 490–496.
6 S. K. Pilli, T. E. Furtak, L. D. Brown, T. G. Deutsch, J. A. Turner and A. M. Herring, *Energy Environ. Sci.*, 2011, **4**, 5028–5034.
7 F. F. Abdi and R. van de Krol, *J. Phys. Chem. C*, 2012, **116**, 9398–9404.
8 J. A. Seabold and K.-S. Choi, *J. Am. Chem. Soc.*, 2012, **134**, 2186–2192.
9 D. Wang, R. Li, J. Zhu, J. Shi, J. Han, X. Zong and C. Li, *J. Phys. Chem. C*, 2012, **116**, 5082–5089.
10 Y. Ma, S. R. Pendlebury, A. Reynal, F. Le Formal and J. R. Durrant, *Chem. Sci.*, 2014, **5**, 2964–2973.
11 F. F. Abdi, L. Han, A. H. M. Smets, M. Zeman, B. Dam and R. van de Krol, *Nat. Commun.*, 2013, **4**, 2195.
12 M. Long, W. Cai, J. Cai, B. Zhou, X. Chai and Y. Wu, *J. Phys. Chem. B*, 2006, **110**, 20211–20216.
13 M. Long, W. Cai and H. Kisch, *J. Phys. Chem. C*, 2008, **112**, 548–554.
14 J. Wang and F. E. Osterloh, *J. Mater. Chem. A*, 2014, **2**, 9405–9411.
15 M. Batzill, *Energy Environ. Sci.*, 2011, **4**, 3275–3286.
16 N. V. Burbure, P. A. Salvador and G. S. Rohrer, *Chem. Mater.*, 2010, **22**, 5823–5830.
17 J. L. Giocondi and G. S. Rohrer, *J. Phys. Chem. B*, 2001, **105**, 8275–8277.
18 L. Li, P. A. Salvador and G. S. Rohrer, *Nanoscale*, 2014, **6**, 24–42.
19 D. Tiwari and S. Dunn, *J. Mater. Sci.*, 2009, **44**, 5063–5079.
20 Y. L. Zhang, A. M. Schultz, P. A. Salvador and G. S. Rohrer, *J. Mater. Chem.*, 2011, **21**, 4168–4174.
21 R. Munprom, P. A. Salvador and G. S. Rohrer, *Chem. Mater.*, 2014, **26**, 2774–2776.
22 P. A. M. Hotsenpiller, J. D. Bolt, W. E. Farneth, J. B. Lowekamp and G. S. Rohrer, *J. Phys. Chem. B*, 1998, **102**, 3216–3226.
23 J. B. Lowekamp, G. S. Rohrer, P. A. M. Hotsenpiller, J. D. Bolt and W. E. Farneth, *J. Phys. Chem. B*, 1998, **102**, 7323–7327.
24 T. Ohno, K. Sarukawa and M. Matsumura, *New J. Chem.*, 2002, **26**, 1167–1170.
25 X. Zhang, Z. Ai, F. Jia, L. Zhang, X. Fan and Z. Zou, *Mater. Chem. Phys.*, 2007, **103**, 162–167.
26 A. W. Sleight, H. Y. Chen, A. Ferretti and D. E. Cox, *Mater. Res. Bull.*, 1979, **14**, 1571–1581.
27 J. D. Bierlein and A. W. Sleight, *Solid State Commun.*, 1975, **16**, 69–70.
28 D. Wang, H. Jiang, X. Zong, Q. Xu, Y. Ma, G. Li and C. Li, *Chem.–Eur. J.*, 2011, **17**, 1275–1282.
29 R. Li, H. Han, F. Zhang, D. Wang and C. Li, *Energy Environ. Sci.*, 2014, **7**, 1369–1376.
30 R. Li, F. Zhang, D. Wang, J. Yang, M. Li, J. Zhu, X. Zhou, H. Han and C. Li, *Nat. Commun.*, 2013, **4**, 1432.
31 J. Yang, D. Wang, X. Zhou and C. Li, *Chem.–Eur. J.*, 2013, **19**, 1320–1326.
32 W. C. Clark and A. G. Vondjidi, *J. Catal.*, 1965, **4**, 691–696.
33 J. M. Herrmann, J. Disdier and P. Pichat, *J. Catal.*, 1988, **113**, 72–81.
34 K. Tanaka, K. Harada and S. Murata, *Sol. Energy*, 1986, **36**, 159–161.
35 J. Torres and S. Cerveramarch, *Chem. Eng. Sci.*, 1992, **47**, 3857–3862.
36 J. L. Giocondi and G. S. Rohrer, *J. Am. Ceram. Soc.*, 2003, **86**, 1182–1189.
37 S. S. Zumdahl and S. A. Zumdahl, *Chemistry*, Houghton Mifflin, Boston, 5th edn, 2000.
38 A. Bhardwaj, N. V. Burbure, A. Gamalski and G. S. Rohrer, *Chem. Mater.*, 2010, **22**, 3527–3534.
39 J. L. Giocondi, P. A. Salvador and G. S. Rohrer, *Top. Catal.*, 2007, **44**, 529–533.
40 T. Luttrell, S. Halpegamage, J. Tao, A. Kramer, E. Sutter and M. Batzill, *Sci. Rep.*, 2014, **4**, 4043.